Journal of Alloys and Compounds 503 (2010) 480–484

Contents lists available at ScienceDirect

Journal of Alloys and Compounds

journal homepage: www.elsevier.com/locate/jallcom

Synthesis, structure, magnetic, optical and Mössbauer properties of $Na_2FeSn(PO_4)_3$

A. El Bouari[a,*], A. El Jazouli[a], S. Benmokhtar[a], P. Gravereau[b], A. Wattiaux[b]

[a] Laboratoire de Chimie des Matériaux Solides, Faculté des Sciences Ben M'Sik, UH2M, Casablanca, Morocco
[b] Institut de Chimie de la Matière Condensée de Bordeaux (ICMCB-CNRS UPR 9048), Université de Bordeaux1, 33608 Pessac, France

ARTICLE INFO

Article history:
Received 26 November 2009
Received in revised form 5 May 2010
Accepted 8 May 2010
Available online 20 May 2010

Keywords:
Nasicon-phosphates
Rietveld
$Na_2FeSn(PO_4)_3$
Magnetic measurements
UV–visible
Mössbauer spectroscopy

ABSTRACT

The phosphate $Na_2FeSn(PO_4)_3$, obtained by solid state reaction, was found to be isotypic with $Na_2CrTi(PO_4)_3$, with space group *R*-3*c* and unit cell parameters $a = 8.6617(2)$ Å, $c = 22.0161(7)$ Å, $V = 1430.47(5)$ Å^3, $Z = 6$. The structural parameters refined using Rietveld method showed that the Na^+ ions occupy totally the M_1 sites and partially the M_2 sites and sharing faces with the $[Sn/FeO_6]$ octahedra. The presence of the unique valence of ferric iron in the reported phosphate was confirmed using UV–visible diffuse-reflectance spectroscopy, magnetic measurements and Mössbauer spectroscopy.

1. Introduction

Inorganic phosphates cover a large class of diverse materials whose applications include: catalysts, solid electrolytes for batteries [1–4], linear and non-linear optical components and laser materials [5–7]. However, the study of phosphates has become more popular particularly, after the development of NASICON groups of fast ionic conductors [8–14]. Original NASICON compounds are solid solutions derived from $NaZr_2(PO_4)_3$ by partial replacement of P by Si, where Na compensates the negatively charged framework, to give the general formula $Na_{1+x}Zr_2P_{3-x}Si_xO_{12}$ ($0 \le x \le 3$). So the general formula of Nasicon materials can be written as $A_xB_y(XO_4)_3$, where A^{n+} can be monovalent cation (Na^+, Li^+, Cu^+,...) or bivalent cation (Ca^{2+}, Ba^{2+}, Cu^{2+},...) and B is one or more ions in tri-, tetra-, or penta-valent state (Fe^{3+}, Cr^{3+},...Ti^{4+}, Zr^{4+},...Nb^{5+}, Sb^{5+},...). The NASICON structure has a negatively charged 3D-framework, where the A^{n+} cations reside in fully or partially occupied sites. The framework is built of $[XO_4]$ tetrahedra linked by corners to $[BO_6]$ octahedra. Each $[XO_4]$ tetrahedron shares each corner with one $[BO_6]$ octahedron and, conversely, each $[BO_6]$ octahedron shares each corner with a different $[XO_4]$ group. The interstitial voids generated within the network are of two types known as M_1 and M_2 sites in the *R*-3*c* space group. A^{n+} ions at the M_1 sites are coordinated by a trigonal antiprism of oxygens and at the M_2 site has a distorted 8-fold coordination. These sites are connected by bottlenecks generally termed M_1M_2 bottlenecks. Specific structural details, such as the size of the M_1M_2 bottleneck [15–17], are needed to understand the electrical parameters (ionic conductivities and activation energies) of these samples. Structural information can be obtained either by single-crystal diffraction or by Rietveld analysis of powder diffraction data.

In general, the properties of the NASICON-type Na^+ ion conductor compounds strongly depend on the chemical stoichiometry, the crystal structure and unit cell parameters, that, at the same time, depend on the ionic radii of the cations located in octahedral (B) and tetrahedral (X) sites. Recently many attempts have been reported on mixed M/M′ phosphates $A_2MM'(PO_4)_3$ (M = Ti^{4+}, Zr^{4+}, Sn and M′ = Fe^{3+}, Cr^{3+}, In^{3+}) on the octahedral site [18–22].

The goal of this work is to synthesize orthophosphate $Na_2FeSn(PO_4)_3$; to refine its crystal structure on the basis of powder data (the Rietveld method). Additionally, the UV–visible diffuse-reflectance spectroscopy, magnetic measurements and Mössbauer spectroscopy have been used to study the valence state of the iron as well as the cation distribution in the compound.

2. Experimental

2.1. Synthesis

Powder of $Na_2FeSn(PO_4)_3$ was prepared by solid state reaction, starting from reagent grade Na_2CO_3, $(NH_4)_2HPO_4$, Fe_2O_3 and SnO_2 mixed in stoichiometric ratios.

* Corresponding author. Fax: +212 522704675.
E-mail address: elbouari@yahoo.fr (A. El Bouari).

0925-8388/$ – see front matter © 2010 Elsevier B.V. All rights reserved.
doi:10.1016/j.jallcom.2010.05.037

Table 1
Structural data and X-ray Rietveld refinement parameters of $Na_2FeSn(PO_4)_3$.

Space group	$R\bar{3}c$
a (Å)	8.6617(2)
c (Å)	22.0161(7)
Volume (Å^3)	1430.47(5)
Wavelength (Å)	$\lambda K_{\alpha1}$ = 1.54060; $\lambda K_{\alpha2}$ = 1.54442
Step scan increment (°2θ)	0.02
2θ range (°)	10–120
Program	FULLPROF
Zero point (°2θ)	−0.045
Pseudo-voigt function [PV = $\eta L + (1-\eta)G$]	η = 0.165(1)
	U = 0.1901(3)
Caglioti law parameters	V = −0.0957(4)
	W = 0.0357(8)
No. of refined parameters	33
R_B	0.05
R_P	0.11
R_{wp}	0.15
χ^2	1.77

The mixture was heated at 200, 600 and finally at 950 °C for 48 h with intermediate grinding. The obtained powder is whitish.

$$Na_2CO_3 + \tfrac{1}{2}Fe_2O_3 + SnO_2 + 3(NH_4)_2HPO_4 \rightarrow Na_2FeSn(PO_4)_3 + 6NH_3 + \tfrac{9}{2}H_2O + CO_2$$

2.2. Instrumental analysis

The X-ray powder diffraction data (XRPD) were collected at room temperature with a Philips PW 3040 (θ–θ) diffractometer using a graphite monochromator. The structure of the iron phosphate compound was derived from the step-scanned X-ray intensity data, in the range 10–120° (2θ) with a step size of 0.02° (2θ) and counting time of 30 s for each step. The structural parameters were refined by Rietveld method [23] using the computer program FULLPROF [24].

Optical absorption spectrum has been recorded at room temperature on a Cary 2400 spectrophotometer in the region 210 and 2400 nm.

Table 2
Atomic coordinates and isotropic temperature factors with their estimated standard deviation E.S.D. corrected with "Berar factor" [25].

Atome	Site	x	y	Z	B_{iso} (Å^2)	Occ
Na(1)	6b	0.0	0.0	0.0	4.43(2)	1
Na(2)	18e	0.6271(2)	0.0	0.25	2.42(2)	1/3
Sn/Fe	12c	0.0	0.0	0.1466(5)	0.30(2)	1
P	18e	0.2903(3)	0.0	0.25	0.11(1)	1
O(1)	36f	0.1855(2)	0.9738(1)	0.1931(4)	0.17(1)	1
O(2)	36f	0.1906(7)	0.1644(6)	0.0865(2)	0.17(1)	1

Magnetic susceptibility measurements were carried out with a Quantum Design SQUID MPMS-5S magnetometer. Data were recorded at a constant applied magnetic field ($0 < H < 3T$) in the temperature range 4.2–340 K.

Mössbauer measurements were performed with a constant acceleration HALDER-type spectrometer using a room temperature ^{57}Co source [Rh matrix] in the transmission geometry. Isomer shift values refer to α-Fe at 293 K. The spectra were recorded at 4.2 and 293 K using a variable temperature cryostat.

3. Structural determination of $Na_2FeSn(PO_4)_3$

3.1. XRPD pattern analysis

The X-ray diffraction pattern can be indexed assuming an hexagonal cell: a = 8.6617(2) Å, c = 22.0161(7) Å. The order of magnitude of these parameters is consistent with a Nasicon-type structure. All the observed reflections could be indexed in the space group R-3c (N° 167). The refinement of the structure was carried out using the Rietveld profilation method. The X-ray diffraction data was collected at room temperature. The initial coordinates were those of $Na_2CrTi(PO_4)_3$ [20]. The sodium was introduced with full occupancy of the M_1 site (one Na atom per formula unit), at (0 0 0) 6b position, and the excess of sodium (one Na atom per formula

Table 3
Interatomic distances (Å) and angles (°) in $Na_2FeSn(PO_4)_3$[a] with their estimated standard deviation E.S.D. corrected with "Berar factor" [25].

(Sn/Fe)O$_6$	O(1)	O(1)	O(1)	O(2)	O(2)	O(2)
O(1)	2.01(2)	2.99(9)	2.99(9)	2.85(7)	4.03(4)	2.87(9)
O(1)	96.36(6)	2.01(2)	2.99(9)	2.87(9)	2.85(7)	4.03(4)
O(1)	96.36(4)	96.36(6)	2.01(2)	4.03(4)	2.87(9)	2.87(7)
O(2)	89.73(5)	90.63(4)	170.13(4)	2.03(7)	2.68(5)	2.68(5)
O(2)	170.13(5)	89.73(4)	90.63(4)	82.43(7)	2.03(7)	2.68(5)
O(2)	90.63(4)	170.13(4)	89.73(5)	82.43(5)	82.42(4)	2.03(7)

Na(1)O$_6$	O(2)	O(2)	O(2)	O(2)	O(2)	O(2)
O(2)	2.45(2)	2.68(5)	2.68(5)	4.91(2)	4.11(3)	4.11(3)
O(2)	66.27(4)	2.45(2)	2.68(5)	4.11(3)	4.91(2)	4.11(3)
O(2)	66.27(3)	66.27(3)	2.45(2)	4.11(3)	4.11(3)	4.91(2)
O(2)	180(3)	113.73(2)	113.73(2)	2.45(2)	2.68(5)	2.68(5)
O(2)	113.73(3)	180(2)	113.73(4)	66.27(2)	2.45(2)	2.68(5)
O(2)	113.73(4)	113.73(3)	180(2)	66.27(3)	66.27(4)	2.45(2)

Na(2)O$_8$	O(1)	O(1)	O(1)	O(1)	O(2)	O(2)	O(2)	O(2)
O(1)	2.88(2)	3.74(3)	3.67(2)	4.52(8)	5.14(2)	4.26(1)	4.44(3)	2.38(4)
O(1)	80.78(4)	2.88(2)	4.52(8)	3.67(2)	4.44(3)	2.38(4)	5.14(2)	4.26(1)
O(1)	83.52(2)	110.61(2)	2.61(1)	5.16(8)	2.87(9)	2.85(7)	3.68(7)	4.15(3)
O(1)	110.61(2)	83.52(2)	161.93(2)	2.61(1)	3.68(7)	4.15(3)	2.87(9)	2.85(7)
O(2)	152.63(3)	113.91(2)	69.86(3)	94.45(4)	2.40(3)	2.68(5)	2.53(8)	4.34(8)
O(2)	108.56(3)	52.98(2)	70.06(2)	113.54(2)	68.85(2)	2.40(3)	4.34(8)	4.60(9)
O(2)	113.91(2)	152.63(3)	94.45(2)	69.86(2)	63.77(2)	132.61(2)	2.34(2)	2.68(5)
O(2)	52.98(3)	108.56(3)	113.54(3)	70.06(2)	132.61(3)	158.53(2)	68.85(2)	2.34(2)

PO$_4$	O(1)	O(1)	O(2)	O(2)
O(1)	1.50(1)	2.53(3)	2.51(2)	2.38(4)
O(1)	115.83(6)	1.50(1)	2.38(4)	2.51(2)
O(2)	111.81(9)	103.42(8)	1.53(2)	2.53(6)
O(2)	103.42(9)	111.81(9)	110.72(6)	1.53(2)

[a] The M–O distances are underlined. O–O distances are given above the diagonal and O–M–O angles are given below.

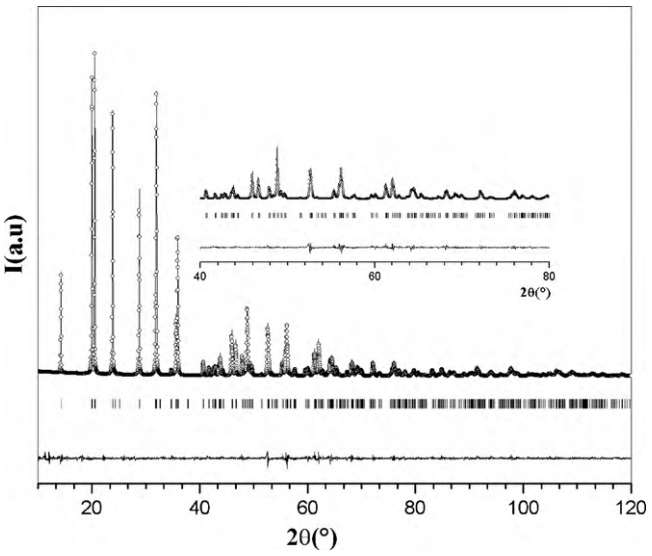

Fig. 1. Observed (. . .), calculated (—) and different powder diffraction patterns of $Na_2FeSn(PO_4)_3$.

unit) located in the M_2 site, 18e position. The iron and tin atoms were assumed to be statistically distributed over the octahedral sites (Nasicon framework). These refinements lead to a rather good agreement between the experimental and calculated XRPD patterns and to follow reliability factors [R_P = 11%, R_{wp} = 15% and R_B = 5%. The experimental conditions of the data collection are given in Table 1. Final atomic coordinates are given in Table 2. Selected interatomic distances and angles are listed in Table 3. The experimental and calculated diffractograms are compared in Fig. 1.

3.2. Structure description

The structure of $Na_2FeSn(PO_4)_3$ consists of a three-dimensional framework of [PO_4] tetrahedra and [(Sn/Fe)O_6] octahedra sharing corners (Fig. 2). The overall set of distances within the framework [(Sn/Fe)–O(1) = 2.01(2) Å, (Sn/Fe)–O(1) = 2.03(7) Å and Na(1)–O(2) = 2.422(4) Å] is in good agreement with the ionic radii values in six coordination [$r(Sn^{4+})$ = 0.69 Å, $r(Fe^{3+})$ = 0.645 Å, $r(Na^{+})$ = 1.02 Å] [26]. The P–O distances [1.50(1) Å; 1.53(2) Å] are comparable to those generally found in Nasicon like phosphate. In M_2 site, the sodium is bounded by eight oxygen with Na(2)–O distance values of 2 × 2.34(2), 2 × 2.40(3), 2 × 2.61(1) and 2.88(2) Å. The Na^+ ions are located in the usually labelled M_1 sites i.e. at the center of an antiprism elongated along the c axis and sharing faces with the (Sn/Fe)O_6 octahedra. The PO_4 tetrahedra are rather regular with a weak angular O–P–O dispersion between 103.42° and 115.83°, around the ideal value 109.45°.

4. Diffuse-reflectance study

Electronic spectrum of $Na_2FeSn(PO_4)_3$ (Fig. 3) was successfully deconvoluted into three Gaussian bands at lower energy, corresponding to crystal field (CF) electronic absorptions at 707, 498 and 418 nm, characteristic of the octahedral environment of Fe^{3+} ions. These bands correspond to forbidden transitions between states with different multiplicities. According to the high-spin d^5 configuration, the fundamental term is $^6A_{1g}(S)$ and the observed bands correspond, respectively to the transitions:

$B_1: {}^6A_{1g}(S) \rightarrow {}^4T_{2g}(G)(707\,nm)$

$B_2: {}^6A_{1g}(S) \rightarrow {}^4T_{1g}(G)(498\,nm)$

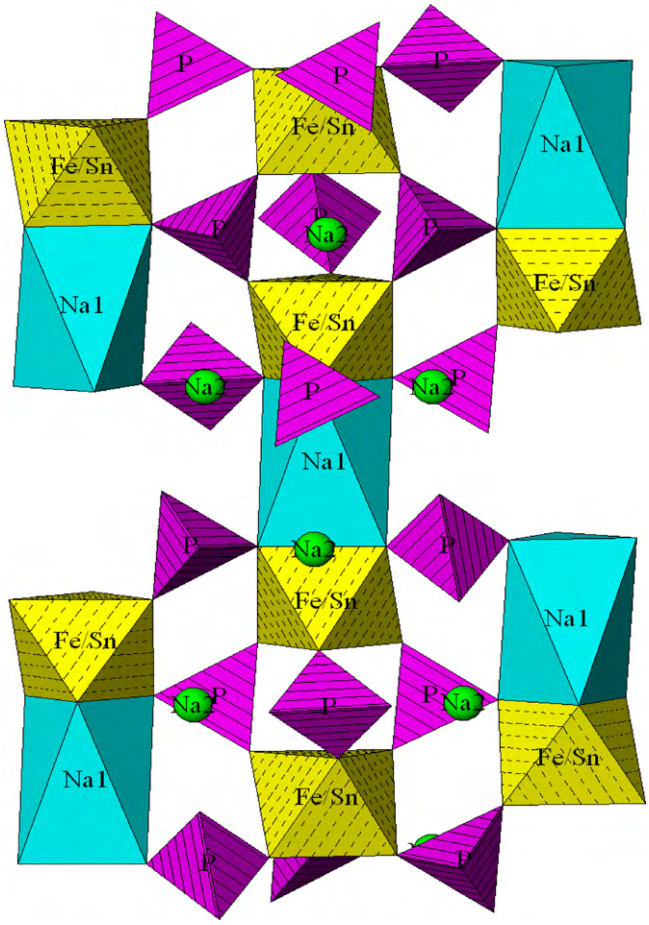

Fig. 2. Structure of $Na2FeSn(PO_4)_3$.

$B_3: {}^6A_{1g}(S) \rightarrow {}^4A_{1g}(G), {}^4E_{2g}(G)(418\,nm)$

Plus two further bands (one Gaussian and one Lorentzian) at higher energy, probably referable to metal-oxygen charge transfer (MLCT). The intense bands observed in the UV region (236 nm, 313 nm) are attributed to O → Sn/Fe charge transfers. Due to the higher oxidant power of the Fe(III) in comparison with Sn(IV), O → Fe charger transfer occurs at lower energy (313 nm) than the O → Sn charger transfer (236 nm).

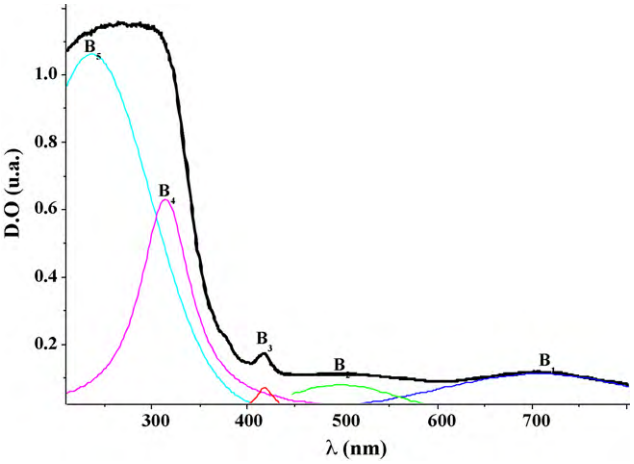

Fig. 3. Diffuse-reflectance spectra of $Na_2FeSn(PO_4)_3$.

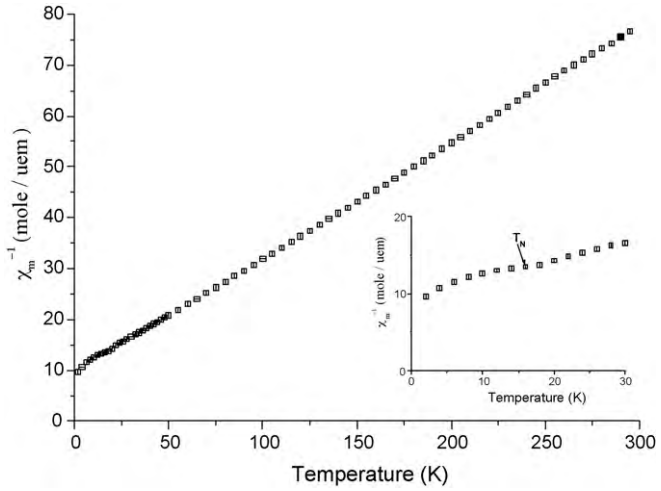

Fig. 4. Reciprocal molar magnetic susceptibility of $Na_2FeSn(PO_4)_3$ as a function of temperature.

5. Magnetic properties

The experimental $\chi_M{}^{-1} = f(T)$ variation (Fig. 4) shows the onset of a long-range antiferromagnetic order at a Neel temperature of 16 K. Above this temperature, the data can be fitted with a Curie Weiss law, $\chi_M{}^{-1} = C/(T-\theta)$, with a Weiss temperature $\theta = -40$ K and a Curie constant $C = 4.35$ emu K mol^{-1}. The negative value of θ reveals the existence of antiferromagnetic interactions between the metallic ions. The value of C is slightly close to the value predicted for high-spin Fe^{3+} ($t_{2g}{}^3e_g{}^2$), in octahedral environment, with only spin contribution (4.375 cm^3 K mol^{-1}) [27].

6. Mössbauer spectroscopy

The Mössbauer spectra of $Na_2FeSn(PO_4)_3$ measured at 293 and 4.2 K are shown in Fig. 5 and Fig. 5a. The experimental data are represented by points and the fitted curves by solid lines. The hyperfine parameters corresponding to the fits are listed in Table 4. The results obtained indicate that the compound is paramagnetic at 293 K and magnetically ordered at 4.2 K.

The Mössbauer spectrum at room temperature indicates the presence of a symmetrical doublet with $\delta = 0.46$ mm/s (isomer shift) in the range 0.29–0.5 mm s^{-1} expected for high spin Fe^{3+} ions in an octahedral field [28–30], and $\Gamma = 0.28$ mm/s (quadrupole splitting). The obtained isomer shift value is compared to the isomer shift values observed in $K_3Fe(PO_4)_2$ [31], $Fe_2(SO_4)_3$ [32] and $Li_3Fe_2(AsO_4)_3$ [33] where their structures are built up from isolated [FeO_6] octahedra linked by the [XO_4] tetrahedra (X = S, P, As) (Table 5); the

Table 4
The Mössbauer parameters of $Na_2FeSn(PO_4)_3$.

$Na_2FeSn(PO_4)_3$	δ (mm/s)	Γ (mm/s)	H (Tesla)
$T = 293$ K	0.46	0.28	–
$T = 4.2$ K	0.55	0.35	50.7

Table 5
The room temperature isomer shift for $Li_3Fe_2(SO_4)_3$, $K_3FePO_4)_2$, $Na_2FeSn(PO_4)_3$ and $Fe_2(SO_4)_3$.

	Compound			
	$Fe_2(SO_4)_3$	$K_3Fe(PO_4)_2$	$Na_2FeSn(PO_4)_3$	$Li_3Fe_2(AsO_4)_3$
δ (mm/s)	0.49	0.46	0.46	0.39
X–O (Å)	1.464	1.533	1.515	1.683
Ref.	[28]	[27]	This work	[29]

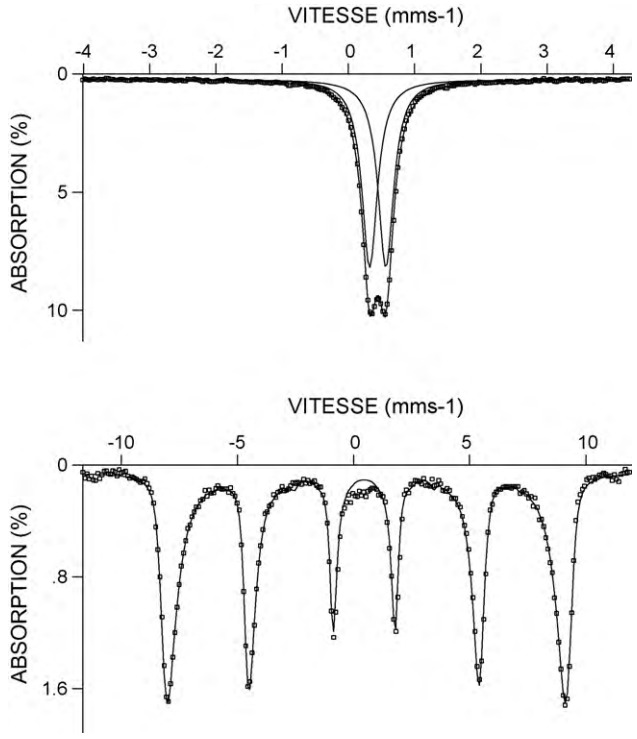

Fig. 5. Mössbauer spectra of $Na_2FeSn(PO_4)_3$ (a) $T = 293$ K, (b) $T = 4.2$ K.

comparison shows that while going from S to P to As containing compounds a decrease in the isomer shift value is observed: $\delta S > \delta P > \delta As$. This trend can be explained by the principle of antagonic bonds. According to this principle, the lengthening of the X–O bond (Table 5) which reasonably increases its ionicity induces an increase of the covalence character of antagonic Fe–O bond, reducing the isomer shift from sulphate to arsenate.

The Mössbauer spectrum at $T = 4.2$ K shows clearly a sextuplet characteristic of the magnetic ordered compound (Fig. 5b) in agreement with the magnetic susceptibility results. The difference between the low temperature and the room temperature isomer shifts is due in part to the second order Doppler effect.

7. Conclusions

Powder of $Na_2FeSn(PO_4)_3$ compound has been prepared by solid state route. Its crystal structure has been resolved by Rietveld method, from powder X-ray diffraction data, the results revealed that the compound is isotypic with $Na_2CrTi(PO_4)_3$ and belongs to the Nasicon family and crystallizes in the in *R*-3*c* space group. It is formed by a 3D network of [Fe/SnO_6] octahedra and [PO_4] tetrahedra connected by corners. Fe^{3+} and Sn^{4+} cations are statistically distributed in the octahedral sites (12c) of the framework. Na occupies totally the M_1 sites and partially the M_2 sites. The oxidation state of irons was clearly identified by Mössbauer spectroscopy, magnetic measurement and UV–visible.

References

[1] L. Tortet, J.R. Gavarri, G. Nihoul, A.J. Dianoux, J. Solid State Ionics 97 (1997) 253.
[2] B. Louati, K. Guidara, M. Gargouri, Phys. Status Solidi B 241 (2004) 1994.
[3] B. Louati, M. Gargouri, K. Guidara, T. Mhiri, J. Phys. Chem. Solids 66 (2005) 762.
[4] J.K. Feng, L. Lu, M.O. Lai, J. Alloys Compd. (2008), doi:10.1016/j.jallcom.2010.04.084.
[5] K. Sasaki, N. Ohno, Nonlinear Opt. 29 (2002) 615.
[6] Jun-Kang Sun, Fu-Qiang Huang, Yao-Ming Wang, Zhi-Chao Shan, Zhan-Qiang Liu, Min-Ling Liu, Yu-Juan Xia, Kai-Qiang Li, J. Alloys Compd. 469 (2009) 327.
[7] I.M. Nagpure, K.N. Shinde, Vinay Kumar, O.M. Ntwaeaborwa, S.J. Dhoble, H.C. Swart, J. Alloys Compd. 492 (1–2) (2010), 384, 4.

[8] T. Fuyuki, K. Sasaki1, N. Ohno, J. Lumin. 112 (2005) 250.
[9] H. Bih, L. Bih, B. Manoun, M. Azdouz, S. Benmokhtar, P. Lazor, J. Mol. Struct. 936 (2009) 147.
[10] Navulla Anantharamulu, K. Koteswara Rao, M. Vithal, G. Prasad, J. Alloys Compd. 479 (1–2) (2009) 684,24.
[11] Essehli Rachid, Brahim El Bali, S. Benmokhtar, Fejfarová Karla, Dusek Michal, Mater. Res. Bull. 44 (2009), 1502, 7.
[12] N. Anantharamulu, R. Velchuri, T. Sarojini, K. Madhavi, G. Prasad, M. Vithal, Indian J. Eng. Mater. Sci. 16 (2009) 347.
[13] T. Masui, K. Koyabu, S. Tamura, N. Imanaka, J. Alloys Compd. 418 (2006) 73.
[14] M. Barre, M.P. Crosnier-Lopez, F. Le Berre, E. Suard, J.L. Fourquet, J. Solid State Chem. 180 (2007) 1011.
[15] H. Kohler, H. Schulz, Solid State Ionics 9–10 (1983) 795.
[16] H. Kohler, H. Schulz, Mater. Res. Bull. 20 (1985) 1461.
[17] H. Kohler, H. Schulz, Mater. Res. Bull. 21 (1986) 23.
[18] R. Perret, J. Less Common Met. 144 (1988) 195.
[19] O. Tillement, J. Angenault, J.C. Couturier, M. Quarton, Solid State Ionics 53–56 (1992) 391.
[20] Sébastien Patoux, Gwenaëlle Rousse, Jean-Bernard Leriche, Christian Masquelier, Chem. Mater. 15 (2003) 2084.
[21] Sébastien Patoux, Gwenaëlle Rousse, Jean-Bernard Leriche, Christian Masquelier, Solid State Sci. 6 (2004) 1113.
[22] Aatiq Abderrahim, Powder Diffr. 19 (3) (2004) 272.
[23] H.M. Rietveld, Acta Crystallogr. 22 (1967) 151.
[24] J. Rodriguez-Carvajal, Collected Abstr. Powder Diffr. Meet. (Toulouse. France) (1990) 127.
[25] J.F. Berrar, P. Lelann, J. Appl. Cryst. 24 (1) (1991) 1.
[26] R.D. Shannon, Acta Crystallogr. A 32 (1976) 751.
[27] C. Kittel, Introduction to Solid State Physics, sixth ed., Wiley, New York, 1986, Vol. 406.
[28] N.N. Greenwood, T.C. Gibb, Mössbauer Spectroscopy, Chapman & Hall, London, 1971, 659.
[29] F. Menil, J. Phys. Chem. Solids 46 (1985) 763.
[30] C. Gleitzer, Eur. J. Solid State Inorg. Chem. 28 (1991) 77.
[31] Besma Lajmi, Mourad Hidouri, Abdel-Karim Ben Hammouda, AlainWattiaux, Léopold Fournés, Jacques Darriet, Mongi Ben Amara, Mater. Chem. Phys. 113 (2009) 372.
[32] G.J. Long, G. Longworth, P. Battle, A.K. Cheetham, R.V. Thundathil, D. Beveridge, Inorg. Chem. 18 (1979) 624.
[33] Z. Jirack, R. Salmon, L. Fournés, F. Menil, P. Hagenmuller, Inorg. Chem. 21 (1982) 4218.